Beyond y-Al2O3crystallite surfaces: The hidden features of edgesrevealed by solid-state1H NMR and DFT calculations

Ana T.F. Batista, Dorothea Wisser, Thomas Pigeon, David Gajan, Fabrice Diehl, Mickael Rivallan, Leonor Catita, Anne-Sophie Gay, Anne Lesage, Céline Chizallet, et al.

Beyond γ-Al_2O_3 Crystallite Surfaces: the Hidden Features of Edges Revealed by Solid-State ^{1}H NMR and DFT Calculations

Ana T. F. Batista [a], Dorothea Wisser [a,b], Thomas Pigeon [a], David Gajan [b], Fabrice Diehl [a], Mickael Rivallan [a], Leonor Catita [a], Anne-Sophie Gay [a], Anne Lesage [b], Céline Chizallet [a], and Pascal Raybaud [a,*]

[a] IFP Energies nouvelles, Rond-point de l'échangeur de Solaize, 69360 Solaize (France)

[b] Centre de RMN À Très Hauts Champs, Université de Lyon (CNRS/ENS Lyon/UCB Lyon 1), 69100 Villeurbanne (France)

Corresponding author: Pascal Raybaud, E-mail address: pascal.raybaud@ifpen.fr

Abstract

Elucidating the nature of high surface area gamma alumina sites is of great interest for numerous applications. In this work, the structural and spectroscopic features of edge sites are unravelled thanks to density functional theory (DFT) calculations combined with high field ^{1}H MAS NMR of two high surface area alumina samples of distinct morphologies. DFT chemical shift calculations were carried out for relevant surface models with different hydration degrees. However, the best assignment is achieved by considering the first DFT model representing the hydroxylated edges located at the intersection of (110) and (100) alumina facets. The sharp ^{1}H NMR peak at 0 ppm corresponds to μ_1-OH groups which are located on this edge and are free from hydrogen bonding. Moreover, we show that these edge sites are the most reactive with respect to chlorine exchange.

Keywords: alumina, density functional theory, edge, hydroxyls, NMR spectroscopy

1. Introduction

The gamma polymorph of Al_2O_3 is used in numerous industrial applications thanks to its remarkable catalytic and adsorptive properties[1] which have been extensively studied by experimental and theoretical approaches.[2–9] In particular, surface hydroxyl groups, responsible for Brønsted acidity, have been characterized by infra-red (IR) spectroscopy [2,3,10–12] and by ^{1}H solid-state nuclear magnetic resonance (NMR) spectroscopy.[12–16] Moreover, DFT calculations[5] enabled the refinement of the empirical assignment of the main IR bands thanks to the determination of the hydration of the three main exposed γ-Al_2O_3 surfaces:[17] (110), (100) and (111). In ^{1}H NMR work, the use of high fields and fast magic angle spinning (MAS) provided improved spectral resolution, revealing various, partially resolved, ^{1}H signals. Three main spectral regions were identified at around 0 ppm, 1-3 ppm and 3-5 ppm, respectively assigned to non H-bonded μ_1-OH; μ_2-OH and μ_3-OH. These hydroxyls are connected to one, two or three Al atoms exhibiting different coordination (Al_{IV}, A_{lV}, Al_{VI}).[15,16] Also, broad signals above 5 ppm were associated with hydrogen bond donor species.[16]

However, to go beyond the current knowledge of high surface aluminas, atomic scale insights into the nature and location of the hydroxyls that originate each signal are required. In particular, considering extended surfaces only to interpret NMR data overlooks that γ-Al_2O_3 crystallites are finite nano-objects exhibiting various morphologies. Like metallic nano-particles with stepped surfaces and edges that provide low coordination sites active in catalysis,[18–21] edge architectures present on alumina crystallites should harbour original hydroxyl and Al sites distinct from those on such surfaces. In a recent review, Busca points to the likely role of edges and corners on alumina's reactivity, which are suspected to be the location of the strongest Lewis acid sites bearing hydroxyl groups more resistant to dehydration.[8,22]

Here, the interpretation of the proton NMR spectra of γ-Al_2O_3 is revisited, providing new insights into the nature and location of the hydroxyls in order to refine our current structural knowledge of high surface area aluminas. ^{1}H NMR spectra was recorded on two Al_2O_3 samples of different morphologies, and it is shown by chemical shift DFT calculations that considering alumina facets only leads to an incomplete description of the spectra. This challenge is solved by establishing edge models highlighting the selective chlorination of the edge sites.

2. Materials and methods

Two relevant commercial high surface alumina samples are considered, PuralSB3 and TH100 (Sasol), labelled *P-egg* and *T-flat* respectively, exhibiting different high BET surfaces (S.I.S1). Their characterization by high-resolution transmission electron microscopy (HR-TEM) suggests that T-flat crystallites are larger and have a better defined and more parallelepipedic platelet-like morphology than P-egg's, which appear to have a round shape (S.I.S1). Chlorinated alumina samples were prepared by exposing alumina to a HCl solution ($3.5\%_w Cl/g_{dry\ alumina}$) for 45 minutes, followed by drying and calcination at 520°C. After thermal treatment under H_2 for 2h at 500°C (ramp 5°C/min) and rotor packing under inert atmosphere, quantitative solid-state ^{1}H NMR spectra were acquired. H SS MAS NMR spectra were obtained on a SB Bruker Avance III 800 (800 MHz ^{1}H resonance frequency, 18.8 T) spectrometer using a zirconia 2.5 mm rotor at 30 kHz MAS. Quantitative ^{1}H spectra were recorded using a DEPTH[23–25] sequence for probe background suppression. Pre-scan delays were set to five times the ^{1}H longitudinal relaxation time (T_1). Chemical shifts were referenced relative to adamantane. Spectral deconvolution was done using DMFit[26]. These spectra recorded at high magnetic field and relatively fast MAS reveal the surface OH signals and subtle changes in chemical shifts between the two different types of alumina (Figure 1 a).

To help for the interpretation of NMR experiments, chemical shifts (S.I.S2.3.) have been calculated by using the linear response approach[27,28] within the PBE-dDsC exchange correlation functional[29,30] and PAW pseudopotentials[31] with an energy cut off of 400 eV as implemented in the VASP code.[32,33] The average of the isotropic chemical shielding (σ) of each proton on a TMS (tetramethylsilane) model (a single molecule surrounded by vacuum) was used as reference to calculate the isotropic chemical shift (δ) of the protons of the various hydroxyls of the alumina surfaces or at the edges :

$$\delta_{iso}=\sigma_{iso}-\sigma_{ref} \qquad (1)$$

For that purpose, relevant periodic models of alumina (110), (100) and (111) surfaces and (110)-(100) edges have been constructed and optimized for various thermodynamically relevant hydration coverages depending on the experimental (T, P) analytical conditions (S.I.S2.). Geometry optimizations were performed using a conjugate-gradient algorithm and convergence criterion on forces of 0.01 eV $Å^{-1}$.

3. Results and Discussion

^{1}H NMR spectra of P-egg and of T-flat (Figure 1 a) present the main features expected for γ-Al_2O_3: a resolved signal at around 0 ppm; intense and well-defined peaks in the 1-3 ppm range and broad components ranging from 3-7 ppm. Moreover, the spectra of the two aluminas are clearly distinguished. The most remarkable difference is that the higher-field signal (at respectively -0.1 and -0.4 ppm) is much more intense for P-egg than for T-flat (12% vs 4% of total ^{1}H signal from spectral deconvolution, Table S2). The 1-3 ppm region is also distinguishable: for P-egg two main signals (1.6 and 2.2 ppm) are observed while for T-flat only one is (1.2 ppm), albeit some shoulders indicating other contributions. Lastly, the contribution of the broad signals ranging from 3-7 ppm is significantly more intense in the T-flat spectrum.

In order to rationalize these experimental results, chemical shifts were calculated (Figure 1 b and S.I.S2.3) for hydrated surface models of the three main exposed γ-Al_2O_3 surfaces[17] (110), (100) and (111) as defined in previous DFT works [4,5,7] For each surface, several hydration degrees were considered (S.I.S2.1.) in order to well represent the alumina samples after thermal treatment, (Figure S8). In the experimental conditions, 10^{-4}< P(H_2O) <10^{-6} bar and 700K< T <800K, the (110) surface exhibits 3.0 OH/nm² and 9.0 OH/nm², the (111) surface 12.3 OH/nm², while the (100) surface is dehydrated.

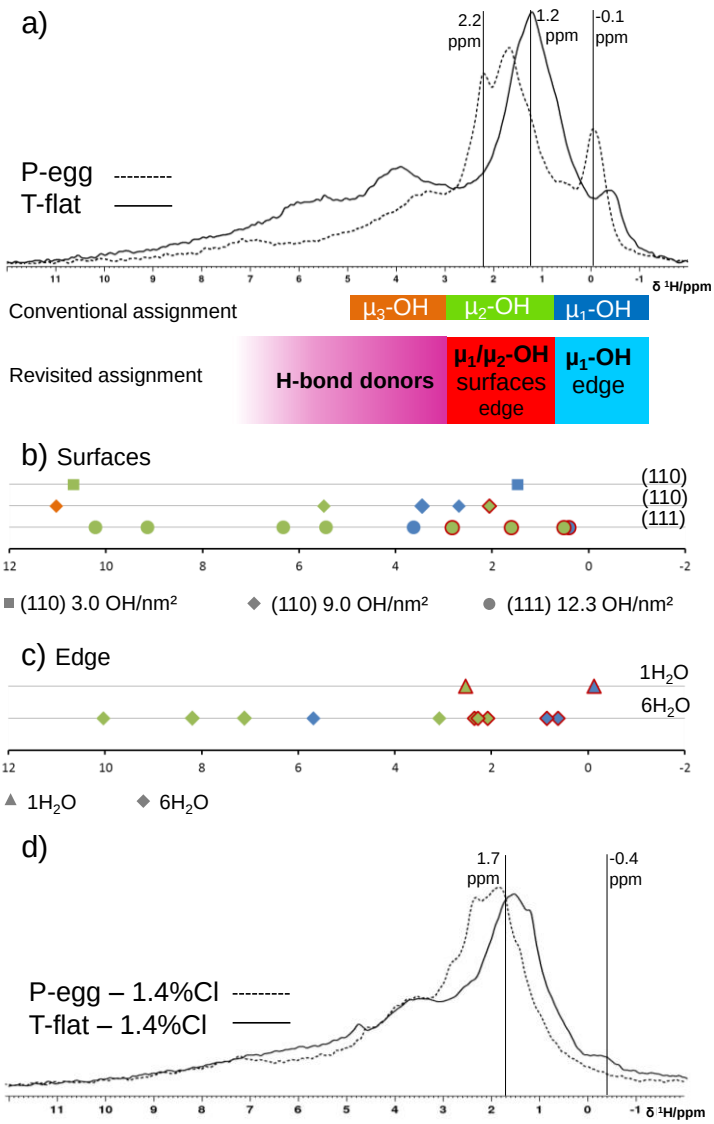

Figure 1. a) ^{1}H MAS NMR spectra of two aluminas with different morphologies, P-egg and T-flat (800 MHz, 30 kHz MAS). The conventional assignment and the revisited one are

represented below. b) ^{1}H chemical shifts calculated by DFT for hydroxyls, colour coded according to the type of OH group given in the conventional assignment, for three surface models; non H-bond donor hydroxyls are highlighted by red outlining. c) ^{1}H chemical shifts calculated by DFT for hydroxyls for the (110)-(100) edge model at two hydration degrees. d) ^{1}H MAS NMR spectra (800 MHz, 30 kHz MAS) of chlorinated samples.

First, it can be noted that most of the hydroxyls on these surfaces are involved in hydrogen bonding (Tables S8, S9, S10). Almost half of them are H-bond donors, resulting in high chemical shifts: several μ_2-OH appearing at >5 ppm. In this case, the chemical shift correlates with hydrogen bond length (Figures S11 and S12),[16,34–36] leading to large variations in δ. Experimentally, H-bond donors are not expected to provide well defined signals such as the ones observed up to 3 ppm.[36]

Thus, we observe a poor correspondence between the previously proposed range and the simulated ^{1}H chemical shifts which do not explain the below 0 ppm signal, expected to correspond to μ_1-OH.[14,15] Contributions calculated at 0.4 and 0.8 ppm from μ_1-OH and μ_2-OH (respectively) of the (111) surface are found, while the classical assignment does not expect μ_2-OH in this range. In addition, no μ_3-OH are predicted in the 3-5 ppm region. Overall, these results show that the resonances observed in the experimental ^{1}H NMR spectra of these γ-Al_2O_3 samples cannot be fully interpreted by considering only their crystalline surfaces. This trend holds true for any hydration degrees (S2.1 and S2.3).

To go beyond, another site architecture must be conceived. Apart from the empirical model proposed by Busca,[8] no atomistic model of alumina edge was previously reported in the literature. Thus, a novel model for the (110)-(100) edge was determined (Figure 2 a) based on a nano-rod structure (S.I.S2.2) resulting from the cleavage of the alumina bulk[37] in the two directions perpendicular to the (110) and (100) surfaces. This induces two edge-terminations,

one exposing Al atoms (here called Al-edge) and the other exposing O atoms (O-edge). The Al-edge is constituted of one upper row of Al_{III} atoms (also three-fold coordinated on the (110) surface) and one lower row of Al_{III} atoms that correspond to Al_{IV} on the (110) surface. The O-edge exhibits a row of alternating O_{II} and O_{III}, both formally O_{III} on the (110) surface. These rows of atoms on both edges will be referenced to as edge sites.

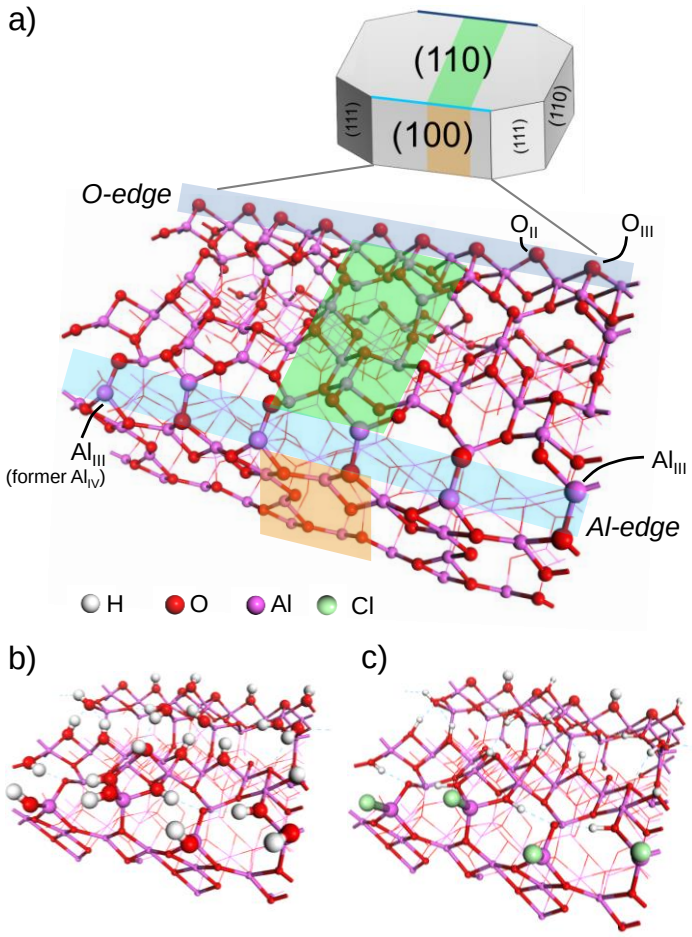

Figure 2. a) Alumina platelet scheme[5] and dehydrated edge model corresponding to two possible edge terminations (blue) between the (110) (green, top) and the (100) (orange, sides) surfaces. Edge sites are depicted by bigger balls. b) hydrated edge model with $6H_2O$ and c) chlorinated edge model constructed from the $6H_2O$ hydrated model by exchanging Al-side μ_1-OH. Blue traced lines indicate hydrogen-bonds (bond length's threshold of 2.5 Å).

The systematic study of the hydration state of the nano-rod (and the corresponding edges) shows that water is the most strongly stabilized at the edge sites, rather than on the facet sites. For the adsorption of the first water molecule per unit cell of simulation, this leads to the formation of one μ_2-OH, the H^+ bonding to the O_{II} atom on the O-edge, and of one μ_1-OH, the OH^- bonding to the Al_{III} on the lower row on the Al-edge that relaxes into a tetragonal geometry (Table S7). Both these hydroxyls are not involved in hydrogen bonding. The corresponding adsorption energy is -436 $kJ.mol^{-1}$, which is far greater than usual adsorption energies reported on the alumina surfaces,[4] and is consistent with the chemical intuition that the reactivity of Lewis Al edge sites should be greater.[8] Such a configuration is a priori striking when thinking in terms of water dissociation, because the hydroxyl and the corresponding proton are not lying on the same kind of edge. However, one shall consider that experimentally, such low hydration states are obtained upon dehydration of the surface sites, making it possible to leave at the surface distant OH and H groups in the end, after recombination of other OH and H pairs. When more than two water molecules are adsorbed per unit cell of simulation, all the "edge sites" are saturated and the near edge sites on the (110) top surface of the nano-rod start being occupied (Figure 2 b), while the (100) facet of the rod remains dehydrated. These "near edge" sites exhibit a H-bond network identical to that of the surface models. In the conditions of thermal treatment (10^{-4}< $P(H_2O)$ <10^{-6} bar and 700K< T <800K), among the multiple hydration degrees equally stable (S.I. Figure S10), we choose two relevant cases: one and six adsorbed water molecules per pair of edges.

The calculated ^1H chemical shifts for the (110)-(100) edge with one and six adsorbed water molecules are represented in Figure 1 c). μ_1 and μ_2 hydroxyls on edge sites appear in the expected δ range: ≈0 ppm and ≈2 ppm respectively. These OH are not only free from hydrogen bonding, but also isolated from other neighbouring hydroxyls. For 6 H_2O

molecules, hydroxyls with δ >3 ppm are located on near edge sites and are H-bond donors, as the red outlining indicates.

With this edge model a significantly improved correlation between experimental and calculated chemical shifts is achieved, especially for the sharp peak at ≈0 ppm. Thus, this peak corresponds mostly to isolated μ_1-OH located on the edges of alumina crystallites, which are free from hydrogen bonding. While the contribution of some free and H-bond acceptor species on the (111) surface cannot be ruled out, their contribution to the signal is minor, as discussed ahead. The 1-3 ppm region is expected to result from non-isolated μ_1-OH and μ_2-OH that are free from H-bonds or H-bond acceptors located on the edges and on the surfaces of the crystallites. The fact that in average, the μ_2-OH sites are much more represented in this region with respect to the 0-1 ppm region, is in agreement with ^{1}H-^{27}Al RESPDOR experiments by Taoufik et al..[15] While not much insight was gained into the 3-5 ppm broad signal, its empirical assignment to μ_3-OH is strongly questioned. Indeed, for the hydration degree of our samples, only two μ_3-OH were found in the models of interest (one for (110) 12.0 OH/nm² and other for edge $6H_2O$) and both are hydrogen bond donors with δ > 5 ppm (7.9 and 14.2 ppm, respectively). Moreover, μ_1-OH and μ_2-OH species acting as hydrogen bond donors are also impacting the 3-5 ppm broad signal. Lastly, broad signals with δ > 5 ppm are thought to correspond to hydroxyls involved in the hydrogen bond network of the surfaces as hydrogen bond donors.

With this improved assignment, it is now possible to rationalize the impact the alumina nano-crystallite morphology on the ^{1}H NMR spectra. As mentioned above, P-egg crystallites are rounded and smaller than those of T-flat, which are more parallelepipedic. Thus, P-egg presents a higher edge to surface ratio than T-flat, which explains the relative intensities of the ≈0 ppm peaks of edge μ_1-OH: 12% and 4% of ^{1}H signal intensity for P-egg and T-flat respectively (Table S2). In the 1-3 ppm region, the δ value of the most intense peak depends

on the sample which is a strong indication of different proportions of exposed surface types for each alumina. Indeed, the electron diffraction analysis (Figure S4) suggests that the (111) termination is more exposed in T-flat crystallites than in P-egg's. Finally, the large signal for $\delta > 3$ ppm is more intense for T-flat, which is explained by a H-bond network between hydroxyls that is more developed on the extended surface planes of T-flat than on P-egg.

To get further insights into the surface structure of P-egg and T-flat, the reactivity of the alumina hydroxyls were probed with chlorine. Chlorinated aluminas are used in many catalytic processes[38] but Cl can also be used as a probe for μ_1-OH.[12,14,39] Chlorinated samples were prepared so as to have 0.5 and 1.4%$_{w/w}$Cl deposited on each alumina (referred as P-egg–x%Cl and T-flat–x%Cl with x=0.5, 1.4). The effect of chlorine on the ^{1}H NMR spectra is clearly different for both aluminas (Figure 1 d and Figure S6). For P-egg, the 0 ppm signal disappears completely, as previously reported,[12,14] while the rest of the spectrum remains unchanged. For T-flat, not only does the 0 ppm signal not disappear completely, but it is also observed an intensity increase in the 3-5 ppm region, associated to an intensity decrease for $\delta > 5$ ppm (Table S2).

According to the DFT OH/Cl exchange energies (S.I. S2.5, Figure 2 c), the edge μ_1-OH sites are predominantly exchanged with chlorine out of all the considered hydroxyls. The subsequent exchanged hydroxyls would be the μ_1-OH of the (110) surface and after that only the μ_1-OH and μ_2-OH sites of the (111) surface. Since the ≈0 ppm peak completely disappears for P-egg, and no impact is observed on the remaining parts of the spectrum, it is believed that only the μ_1-OH located on the edges are exchanged with chlorine at 1.4%Cl and not those of the surfaces. For T-flat, since the peak at ≈0 ppm does not fully disappear while the 3-5 ppm and $\delta > 5$ ppm regions are perturbed, not only the edge μ_1-OH are exchanged but also surface hydroxyls (most likely on the (110)), disturbing the H-bond network. The signal remaining at ≈0 ppm after chlorination should correspond to the (111) surface μ_1 and μ_2 hydroxyls. Just as

the electron diffraction analysis, the NMR results also suggest that the (111) surface is relatively more exposed in T-flat crystallites than in P-egg's. This implies that the number of edge μ_1-OH of T-flat is not sufficient to exchange 1.4% Cl while it is the case on P-egg.

4. Conclusion

The construction of the first DFT model of γ-Al_2O_3 crystallite (110)-(100) edge has allowed a refined ^{1}H NMR peak assignment. It was found that the sharp peak at 0 ppm corresponds mostly to μ_1-OH located on the edges of the crystallites that are isolated and free from hydrogen bonding. These hydroxyls are also the most favourably exchanged with chlorine, which can be considered as a selective probe of alumina edges. Overcoming the simple empirical assignment, the 1-3 ppm region corresponds to signals from not only μ_2-OH but also from μ_1-OH located either on the surfaces or on the edge, and that are either H-bond acceptors or free hydroxyls. Moreover, hydroxyls that are hydrogen bond donors are abundant on the surfaces and contribute to the high chemical shift broad signals. Hopefully, this novel alumina edge model and the improved assignment open new perspectives to further explore the potential of the edge sites present in industrially relevant high surface alumina crystallites.

Acknowledgements

A.T.F.B. thanks A.-L. Taleb for her collaboration in HR-TEM analysis and E. Rosati, C. Guegan and C. Mancia for their contribution to sample preparation. M. Marsman (University of Vienna) is acknowledged for advice with respect to chemical shift calculations, and K. Larmier for preliminary computational investigations. Calculations were performed using HPC resources from GENCI-CINES (Grant A0020806134) and from IFP Energies nouvelles. TGIR RMN THC (FR3050 CNRS) is acknowledged for the NMR characterizations.

This work was funded by IFPEN and financial support from Equipex contract ANR-10-EQPX-47-01 is acknowledged. This work was supported by the LCR "CARactérisation des Matériaux pour l'Energie" (CARMEN), IFPEN/CNRS/UCBL/ENS Lyon/UNISTRA/Sorbonne Université, and is part of the "RatiOnAl Design for CATalysis" (ROAD4CAT) industrial chair, project IDEXLYON funded by the French National Research Agency (ANR-16-IDEX-0005).

References

[1] P. Euzen, P. Raybaud, X. Krokidis, H. Toulhoat, J.-L. Le Loarer, J.-P. Jolivet, C. Froidefond, in: F. Schuth, K. S. W. Sing, J. Weitkamp (Eds.), Handbook of Porous Solids, Wiley-VCH Verlag GmbH, Weinheim, Germany, 2002, p. 1591.

[2] H. Knözinger, P. Ratnasamy, Catal. Rev. - SCI. Eng. 17 (1978) 31.

[3] G. Busca, V. Lorenzelli, G. Ramis, R.J. Willey, Langmuir 9 (1993) 1492.

[4] M. Digne, P. Sautet, P. Raybaud, P. Euzen, H. Toulhoat, J. Catal. 211 (2002) 1.

[5] M. Digne, P. Sautet, P. Raybaud, P. Euzen, H. Toulhoat, J. Catal. 226 (2004) 54.

[6] J.H. Kwak, J. Hu, D. Mei, C.-W. Yi, D.H. Kim, C.H.F. Peden, L.F. Allard, J. Szanyi, Science 325 (2009) 1670.

[7] R. Wischert, C. Copéret, F. Delbecq, P. Sautet, Angew. Chem. Int. Ed. 50 (2011) 3202.

[8] G. Busca, Catal. Today 226 (2014) 2.

[9] M. Lagauche, K. Larmier, E. Jolimaitre, K. Barthelet, C. Chizallet, L. Favergeon, M. Pijolat, J. Phys. Chem. C 121 (2017) 16770.

[10] C. Morterra, G. Magnacca, Catal. Today 27 (1996) 497.

[11] A. Zecchina, E. Escalona Platero, C. Otero Arean, Inorg. Chem. 27 (1988) 102.

[12] A. Kytokivi, M. Lindblad, J. Chem. Soc. Faraday Trans. 91 (1995) 941.

[13] E. C. DeCanio, J. C. Edwards, J. W. Bruno, J. Catal. 148 (1994) 76.

[14] J. Hietala, A. Root, P. Knuuttila, J. Catal. 150 (1994) 46.

[15] M. Taoufik, K.C. Szeto, N. Merle, I. Del Rosal, L. Maron, J. Trebosc, G. Tricot, R.M. Gauvin, L. Delevoye, Chem. Eur. J. 20 (2014) 4038.

[16] M. Delgado, F. Delbecq, C.C. Santini, F. Lefebvre, S. Norsic, P. Putaj, P. Sautet, J.-M. Basset, J. Phys. Chem. C 116 (2012) 834.

[17] P. Nortier, P. Fourre, A.M. Saad, O. Saur, J.C. Lavalley, Appl. Catal. 61 (1990) 141.

[18] M. Mavrikakis, P. Stoltze, J.K. Nørskov, Catal. Lett. 64 (2000) 101.

[19] D.W. Blakely, G.A. Somorjai, J. Catal. 42 (1976) 181.

[20] G. A. Somorjai, D. W. Blakely, Nature 258 (1975) 580.

[21] R.A. van Santen, M. Neurock, S.G. Shetty, Chem. Rev. 110 (2010) 2005.

[22] Guido Busca, Progress in Materials Science 104 (2019) 215.

[23] M.R. Bendall, D.T. Pegg, Magn. Reson. Med. 2 (1985) 91.

[24] D.G Cory, W.M Ritchey, J. Magn. Reson. 80 (1988) 128.

[25] M Robin Bendall, Roy E Gordon, J. Magn. Reson. 53 (1983) 365.

[26] D. Massiot, F. Fayon, M. Capron, I. King, S. Le Calvé, B. Alonso, J.-O. Durand, B. Bujoli, Z. Gan, G. Hoatson, Magn. Reson. Chem. 40 (2002) 70.

[27] C.J. Pickard, F. Mauri, Phys. Rev. B 63 (2001) 245101.

[28] J.R. Yates, C.J. Pickard, F. Mauri, Phys. Rev. B 76 (2007) 24401.

[29] J.P. Perdew, K. Burke, M. Ernzerhof, Phys. Rev. Lett. 77 (1996) 3865.

[30] S.N. Steinmann, C. Corminboeuf, J. Chem. Theory Comput. 7 (2011) 3567.

[31] G. Kresse, D. Joubert, Phys. Rev. B 59 (1999) 1758.

[32] G. Kresse, J. Hafner, Phys. Rev. B 49 (1994) 14251.

[33] G. Kresse, J. Furthmüller, Comp. Mater. Sci. 6 (1996) 15.

[34] M. Hunger, Catal. Rev. - SCI. Eng. 39 (1997) 345.

[35] V. M. Gun'ko, V. V. Turov, Langmuir 15 (1999) 6405.

296 [36] C. Chizallet, G. Costentin, H. Lauron-Pernot, M. Che, C. Bonhomme, J. Maquet, F.
297 Delbecq, P. Sautet, J. Phys. Chem. C 111 (2007) 18279.
298 [37] X. Krokidis, P. Raybaud, A.-E. Gobichon, B. Rebours, P. Euzen, H. Toulhoat, J. Phys.
299 Chem. B 105 (2001) 5121.
300 [38] C. Marcilly, in: C. Marcilly (Ed.), Acido-basic catalysis: Application to refining and
301 petrochemistry, Editions Technip, Paris, 2006, p. 101.
302 [39] M. Digne, P. Raybaud, P. Sautet, D. Guillaume, H. Toulhoat, J. Amer. Chem. Soc. 130
303 (2008) 11030.